ChemPubSoc Europe

DOI: 10.1002/syst.201900044

CHEMSYSTEMSCH Communications

Special Collection

Dynamic Vesicles Formed By Dissipative Self-Assembly

Caren Wanzke,[a] Alexander Jussupow,[a] Fabian Kohler,[b] Hendrik Dietz,[b, c] Ville R. I. Kaila,[a] and Job Boekhoven*[a, c]

Synthetic lipid membranes have served as important models for cellular membranes. However, these static membranes do not recapitulate the dynamic nature of the biological membranes which are frequently remodeled to support cellular function. An ideal membrane model would thus also display dynamic exchange of lipids. In this work, we achieve such a system by coupling the self-assembly of peptides into membranes with a chemical reaction cycle. The reaction cycle activates and deactivates the peptides for self-assembly at the expense of a chemical fuel. The resulting membranes are dynamically remodeled, and, over their 40 min lifetime, they emerge, grow, and are torn apart before they eventually decay.

Phospholipids are the main component of biological membranes.[1] Synthetic analogues of these phospholipids have gained significant attention over the past decades as they are ideal model systems for the biological cell membranes.[2,3] However, a crucial difference between synthetic phospholipid membranes and biological ones lies in their dynamics, *i.e.,* synthetic phospholipid membranes are static with low lipid-exchange rates in part due to the low solubility of phospholipids, whereas biological membranes are dynamic. In the cell, new phospholipids are continuously synthesized in the Kennedy pathway while reactions in the Lands cycle remodel existing lipids.[4] Both cycles are non-equilibrium processes that allow the cell to control its membrane morphology, to sustain its asymmetry, and remodel it on demand. A better model system for membranes would thus also include some degree of the dynamics in the building block activation and deactivation. Such a model could be used to explore fundamental mechanisms in biological membrane remodeling or serve as the basis for synthetic cells.

To reconstitute the dynamic behavior of biological assemblies, researchers have previously coupled chemical reactions with a dynamic equilibrium to the activation and deactivation of membrane-forming surfactants yielding so-called dynamic covalent surfactants. For example, the dynamic imine formation from aldehydes and amines was explored to create double-tailed cationic surfactants, *in situ.* This approach resulted in the formation of dynamic micelles, vesicles, and vesicle gels.[5–8] The dynamics were recapitulated in the rapid response of the membranes to changes in their environment.[9,10] Others have introduced the use of lipid-like peptides and other building blocks that self-assemble into bilayers as a model for dynamic membranes.[11–14]

Another approach to the creation of dynamic assemblies which researchers have explored is the use of dissipative self-assembly. In this form of non-equilibrium self-assembly, the dynamics of the assembly process are regulated by fuel-driven chemical reaction cycles.[15–18] The reaction cycle comprises a minimum of two reactions, *i.e.,* an activation reaction and a deactivation reaction (Scheme 1a). In the activation, fuel is irreversibly consumed to convert a precursor into a product. In the deactivation, the activated product is spontaneously reverted to the precursor, typically by solvolysis or reaction with a ubiquitous species in the solvent. In its finite lifetime, the metastable product is capable of self-assembly, resulting in dynamic assemblies that exchange building blocks rapidly and remodeling dynamics regulated by the kinetics of the reaction cycle. For example, in the dissipative self-assembly of fibers,[19] behavior reminiscent of dynamic instabilities in microtubules[20,21] and oscillatory behavior between morphologies[22] has been observed. Other examples of recently described dissipative assemblies include active droplets,[23] hydrophobic colloids,[24] autocatalytic micelles,[46] the formation of clusters of nanoparticles,[25,26] DNA-based hydrogels[27,28] and supramolecular polymers.[29,30] Finally, transient vesicles may be formed by an ATP-hydrolyzing reaction cycle.[31]

In this work, we describe the dissipative assembly of vesicles driven by a reaction cycle that hydrolyzes a carbodiimide. We find that the emerging vesicles are highly dynamic and remodel through several morphologies in their limited lifetime before eventually succumbing to the inevitable decay that comes with reinstating equilibrium. We quantitatively understand the kinetics of the reaction cycle and demonstrate mechanistic insights in how the kinetics affect the self-assembly.

The precursor in our reaction cycle has a C-terminal aspartic or glutamic acid, such that it carries two carboxylates: one on the C-terminus and one on its side group. These carboxylates

[a] C. Wanzke, A. Jussupow, Prof. Dr. V. R. I. Kaila, Prof. Dr. J. Boekhoven
Department of Chemistry
Technical University of Munich
Lichtenbergstrasse 4, 85748 Garching (Germany)
E-mail: job.boekhoven@tum.de
[b] F. Kohler, Prof. Dr. H. Dietz
Physik Department
Technical University of Munich
Am Coulombwall 4a, 85748 Garching (Germany)
[c] Prof. Dr. H. Dietz, Prof. Dr. J. Boekhoven
Institute for Advanced Study
Technical University of Munich
Lichtenbergstrasse 2a, 85748 Garching (Germany)

Supporting information for this article is available on the WWW under https://doi.org/10.1002/syst.201900044

An invited contribution to a Special Collection on Fuelled Self-Assembly

© 2019 The Authors. Published by Wiley-VCH Verlag GmbH & Co. KGaA. This is an open access article under the terms of the Creative Commons Attribution License, which permits use, distribution and reproduction in any medium, provided the original work is properly cited.

© 2019 The Authors. Published by Wiley-VCH Verlag GmbH & Co. KGaA

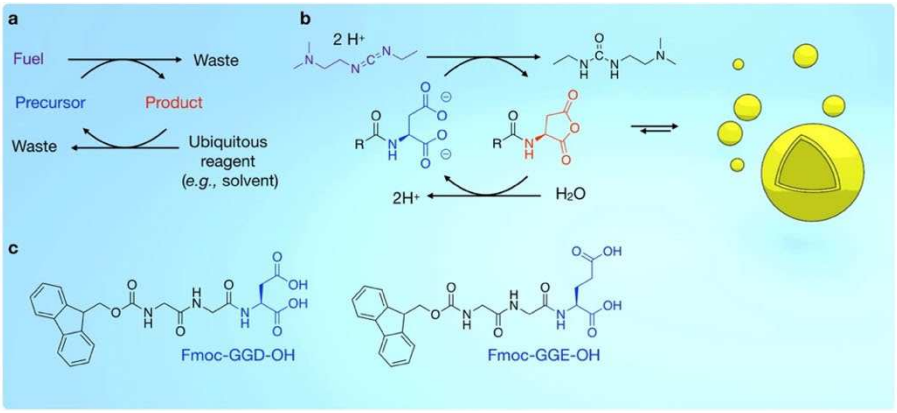

Scheme 1. Description of the chemical reaction cycle and reactants. a) The general design of a fuel-driven chemical reaction cycle. An activation reaction converts a precursor in a product driven by the irreversible consumption of fuel. A ubiquitous reactant, such as a molecule of solvent, spontaneously reacts with the product to yield the precursor; b) The reaction cycle we use to drive dissipative vesicles hydrolyzes a molecule of EDC (fuel) to EDU (waste) to form a transient anhydride; c) The chemical structures of the precursors used in this study.

can be condensed into their corresponding cyclic anhydride at the expense of a carbodiimide fuel (Scheme 1b).[32,33] The conversion to the anhydride constitutes the activation reaction. As a fuel, we used EDC (1-ethyl-3-(3-dimethylaminopropyl) carbodiimide) which was irreversibly converted into its corresponding urea (waste). The cycle was carried out in water, and the anhydride thus hydrolyzed back to the precursor state. The latter reaction is the cycle's deactivation step. As precursors, we used the peptides Fmoc-GGD-OH and Fmoc-GGE-OH, in which Fmoc means fluorenyl-methyloxycarbonyl, G stands for glycine, D and E stand for aspartic and glutamic acid (Scheme 1c). These tripeptides were prepared on a 0.1 gram scale using solid phase peptide synthesis and preparative HPLC (high-performance liquid chromatography). The peptide purity was assessed by analytical HPLC, mass-spectroscopy and NMR (Table S1 and Figures S1, S2, S3). The precursor was dissolved at 10 mM in 200 mM MES buffer at pH 6.0. Both precursors were well-soluble at this concentration.

Upon addition of 100 mM of EDC to the solution of 10 mM Fmoc-GGD-OH, the initially transparent solution turned turbid within seconds. Importantly, the turbidity was a transient phenomenon: it rapidly increased and then decayed over 15 minutes until the original transparency was restored (Figure 1a). The turbidity was quantified by tracing the absorbance at 500 nm wavelength, which confirmed the rapid increase and decay (Figure 1b). The turbidity was less pronounced and persisted for a shorter period when 50 mM EDC was added instead of 100 mM. The same experiments with Fmoc-GGE-OH as precursor resulted in a similar transient increase in turbidity (Figure 1c). Here, the turbidity reached lower levels but persisted for longer compared to Fmoc-GGD-OH. The emergence and decay of turbidity for both precursors upon application of EDC indicates a fuel-driven dissipative self-assembly process that leads to the formation of micrometer-scale light-scattering particles. This dissipative self-assembly process could be repeated up to three times with an addition of 50 mM EDC each before the turbidity started to fade because of the high waste concentration (Figure S4).

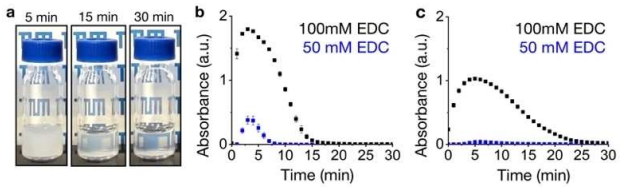

Figure 1. Macroscopic assessment of the dissipative assemblies. a) Photographs of the 10 mM Fmoc-GGD-OH fuelled with 100 mM EDC. The absorbance of 500 nm light as a function of time of b) 10 mM Fmoc-GGD-OH or c) 10 mM Fmoc-GGE-OH fuelled with 50 or 100 mM EDC. The error bar depicts the standard deviation from the average ($n = 3$).

We used confocal laser scanning microscopy to study the nature of the transient assemblies. We added 2.5 μM of the hydrophobic dye Nile Red to a solution of 10 mM Fmoc-GGD-OH. Then, we added 100 mM EDC, to start the reaction cycle, and, every 30 seconds, we imaged the solution (Figure 2a). In the first minutes, microscopy revealed mostly spherical assemblies, with a radius in the range of 0.5 μm. Due to their small size, confocal microscopy could not resolve the exact nature of the assemblies, *i.e.,* whether they were small vesicles, colloids or droplets. After four minutes, we observed large vesicles as well as the small spherical assemblies. The large vesicles had a radius of several micrometers and we could resolve the membrane and inner compartment by confocal microscopy (Figure 2b). As time progressed, the number of these large vesicles started to increase. After 11 minutes, the number of large vesicles and smaller particles decreased until most of them had disappeared after 20 minutes. In this period, we also observed that the vesicles often had defects in the membrane (Figure 2b, white arrow).

The imaging experiments were performed in triplicate which yielded sufficient data to quantify the number of assemblies and their radii by image analysis software. The number of particles rapidly increased after the addition of the

© 2019 The Authors. Published by Wiley-VCH Verlag GmbH & Co. KGaA

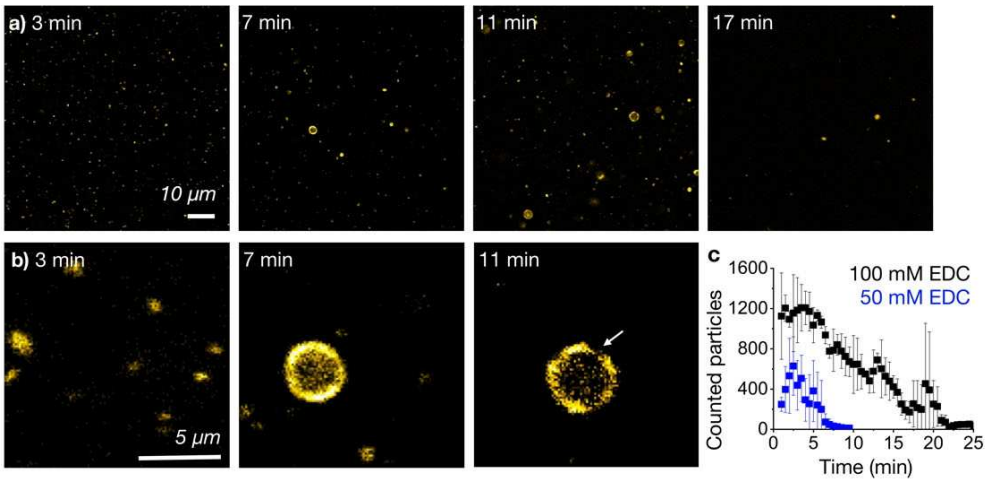

Figure 2. Microscopic assessment of the dissipative assemblies. a) Confocal micrographs of the assemblies formed by the addition of 100 mM EDC to 10 mM of Fmoc-GGD-OH. The time after the addition of EDC is indicated; b) Magnification of the micrographs as described in (a). The white arrow indicates defects in the membrane; c) The number of counted particles per micrograph (250×250 μm) as a function of time. The error bar depicts the standard deviation from the average ($n=3$).

fuel. The maximum number of particles was reached after approximately 5 minutes, after which it decayed to close to zero in 20 minutes (Figure 2c). For Fmoc-GGD-OH fuelled with 50 mM EDC, we also found small spherical assemblies, but much fewer large vesicles (Figure S5). Finally, we performed a confocal microscopy study on 10 mM Fmoc-GGE-OH, fuelled with 100 mM EDC (Figure S6). We observed small spherical assemblies that could not be resolved as well as larger vesicles.

Cryogenic transmission electron microscopy (cryo-TEM) revealed that the small spherical assemblies we observed by confocal microscopy were vesicles (Figure 3). The vesicles had a radius in the range of several 100 nm, were multilamellar, and had a rugged membrane (Figure 3b). Smaller (*i.e.,* 50–100 nm) vesicles were often observed in the proximity of the large multilamellar ones (Figure 3a, black arrows). After 3 minutes of incubation with EDC, vesicles had a rugged membrane and where somewhat larger than the vesicles observed after 1 minute. After 5 minutes, the vesicles were again larger, but the ruggedness mostly smoothed out. Some vesicles had perforated membranes. After 7 minutes, the membranes looked smooth, and the holes in the membrane were less obvious. After 12 minutes, some of the vesicles had deflated, and what remained was the disrupted membranes (Figure S7). We cannot rule out that the deflation of the vesicles is a side effect from EM grid preparation. For Fmoc–GGE–OH fuelled with 100 mM EDC, we also performed a cryo-EM study and found similar results (Figure S8).

We studied the kinetics of the reaction cycle of 10 mM Fmoc-GGD-OH and 100 mM EDC by analytical HPLC and ^{1}H-NMR. We followed the concentration of Fmoc-GGD-OH, its corresponding anhydride and the concentration of EDC over time by HPLC. The EDC concentration decayed throughout 40 minutes (Figure S9a). The intermediate O-acyl urea was not observed, which we previously explained by its rapid conversion to the anhydride.[32] Indeed, the concentration of anhydride rapidly increased in the first minutes after EDC addition (Figure S9b). After four minutes, the anhydride concentration started to decrease. The decrease in anhydride concentration meant that deactivation of anhydride was now faster than its activation. Finally, no significant amount of anhydride was detected after 40 min.

We could predict the evolution of the chemical reaction cycle quantitatively with a previously described kinetic model.[23,32,34] The model calculates the concentration of each reactant every second in an experiment (Supporting notes 1). We used datasets from four HPLC experiments to fit the rate constants in the model. In all the experiments, the precursor concentration was kept at 10 mM, but between experiments, we varied the concentration of EDC from 25 to 100 mM (See Figure S9a–b and Table S4 for the k-values). For Fmoc-GGE-OH, we performed similar experiments (Figure S9c–d). The model describes the observed evolution of the concentration anhydride and EDC accurately (Figure 4a and S9a–d) and provides us with valuable insight into the dynamic evolution of the reaction cycle. For example, the model clarified that over the entire time when vesicles were found, the reaction cycle was dynamically operating, i.e., activation and deactivation of building blocks was happening simultaneously which likely explains the dynamic evolution of the vesicles. Another insight was that we could fit the data with one set of rate constants, independent of whether assemblies were present or not (e.g., 100 mM or 25 mM EDC). Through that observation, we conclude that the rate constants are not affected by the assembly process, which in turn means that hydrolysis is likely to happen both in solution or on the vesicles at equal rates.

We hypothesized that the anhydride product co-assembled with molecules of the anionic precursor. To test the hypothesis, we measured the chemical composition of the vesicle membranes by a ^{1}H-NMR spectroscopy study. We used the fact that molecules in a self-assembled state have a reduced transversal

© 2019 The Authors. Published by Wiley-VCH Verlag GmbH & Co. KGaA

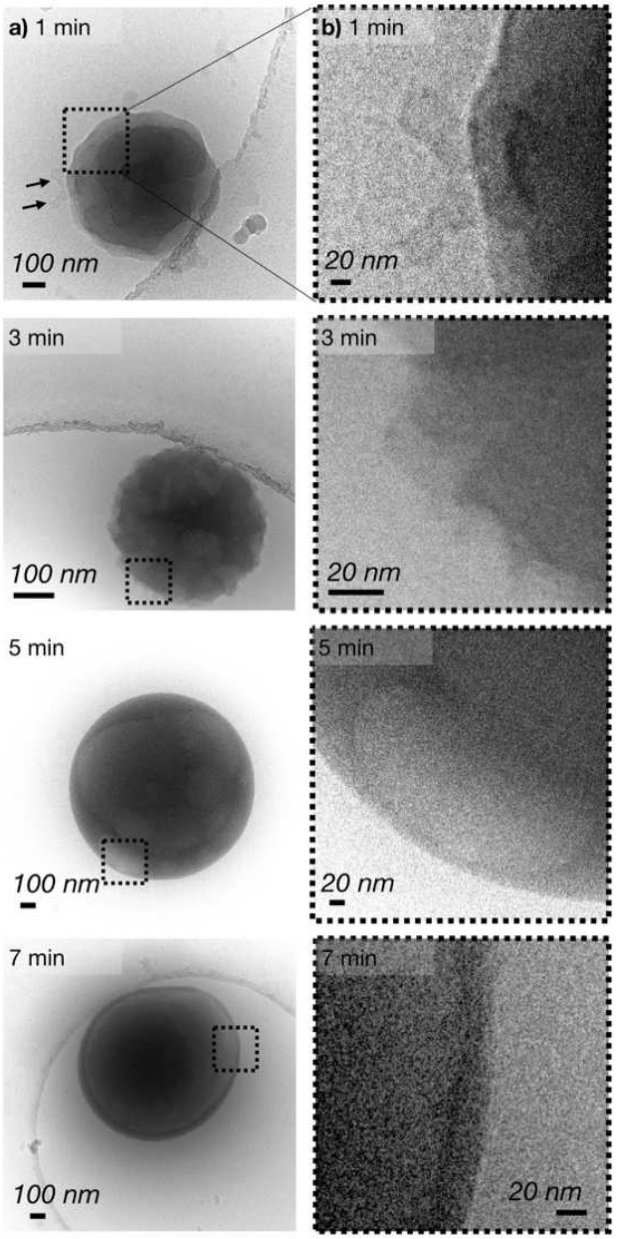

Figure 3. Microscopic assessment of the dissipative assemblies. a) Electron micrographs of the assemblies formed by the addition of 100 mM EDC to 10 mM of Fmoc–GGD–OH. The time after the addition of EDC is indicated. b) Magnification of the micrographs as described in (a).

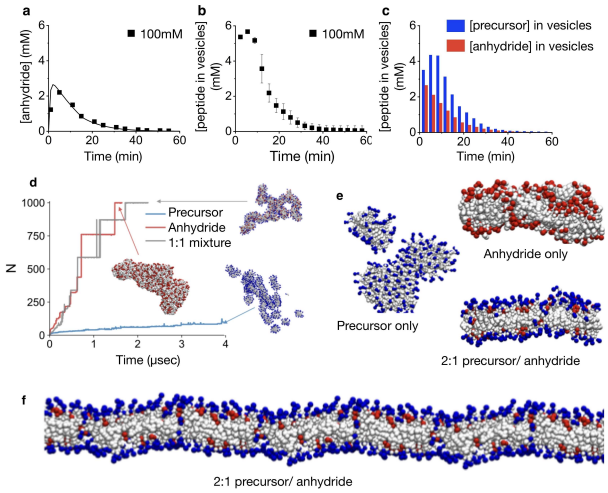

Figure 4. Kinetics and dynamics of the self-assembly process. a–c) Kinetic analysis of a sample of 10 mM Fmoc–GGD–OH fuelled with 100 mM EDC. a) The concentration anhydride against time as measured by HPLC (black markers) and calculated by the kinetic model (black line); b) The concentration peptide in an assembled state as measured by NMR; c) The concentration of precursor and product in the vesicles as a function of time; d–f) Molecular simulations of the Fmoc–GGD–OH; d) The weight-based average size of the assemblies over time. Structures of a finite (e) and infinite (f) preorganized bilayer after 5 μs of MD simulations.

relaxation time (T2) which results in long correlation times followed by a broadening of the signal that gets hidden under the baseline. In other words, molecules that were part of the assembly became NMR-silent, while molecules that remained in solution were NMR-visible. That contrasts the HPLC data which measured the precursor and product concentration independent of their participation in the assembly.

Early in the cycle, the majority of the peptide was not visible by NMR spectroscopy and thus in the assemblies (Figure 4b). Even though the model predicted a maximum concentration of 2.7 mM of the anhydride product, as much as 6 mM of the peptide was observed in the assemblies. From the NMR and kinetic model data, we can calculate the amount of precursor in the assembled state with the following Equation (1):

$$[\text{peptide}]_{\text{in vesicles}} - [\text{product}] = [\text{precursor}]_{\text{in vesicles}} \quad (1)$$

In the calculation, we assume that all the product (anhydride) is in the assemblies. The calculations show that over the entire cycle, the majority of the peptide in the vesicles is the dicarboxylate precursor (Figure 4c). The precursor in the assemblies may have either co-assembled with the product or remained in the assembly after hydrolysis of the product. The latter mechanism seems more likely given the fast hydrolysis rate of the anhydride (with a half-life of less than 1 minute, Table S4) and the fact that hydrolysis happens in solution and on the assemblies.

To further probe the molecular assembly mechanisms of the Fmoc–GGD–OH in the precursor and product forms, we performed coarse-grained molecular dynamics simulations (see Methods). We observed that both the precursor and product self-assembled and that the final structure strongly depended on the ratio of the anionic precursor and neutral product (Figure 4d–e). The precursor spontaneously assembled into small clusters of roughly 100 precursor molecules in the simulated setup (Figure 4d). The growth of larger assemblies was inhibited by the strong intermolecular electrostatic repulsion between the precursor molecules. In contrast, the anhydride product and mixtures of the product and precursor were able to spontaneously form larger assemblies. However, spontaneous formation of membranes was not observed, which is

© 2019 The Authors. Published by Wiley-VCH Verlag GmbH & Co. KGaA

probably due to the limited timescale of the simulation and the size of the simulated system.

Encouraged by the spontaneous self-assembly observed in the simulations, we studied the stability of pre-assembled finite bilayers with different chemical compositions as a prerequisite for the later vesicle formation process. Guided by the unbiased simulations described above, we organized the bilayer such that the hydrophobic Fmoc-groups of the precursor and product were pointing inwards, while the C-terminal residue was pointing towards the aqueous phase. We found that the bilayer was unstable and disassembled on hundreds of nanosecond timescales when it exclusively comprised the precursor (Figure 4e). In contrast, in simulations with one-third of the bilayer building blocks in the anhydride product state, the membrane remained stable on microsecond timescales. These results are also consistent with simulations on a pre-assembled membrane without border effects (Figure 4f). Finally, we found that membranes comprising exclusively product were unstable (Figure 4e and S10). The combined observations suggest there is a subtle balance between attractive and repulsive forces that need to be matched in order to form stable bilayers.

The combined data allowed us to create a tentative mechanism for the dynamic assembly of the vesicles driven by the hydrolysis of EDC (Scheme 2). Before the addition of EDC, no assemblies were present. Also, an hour after the addition of EDC, no assemblies were present. Both observations imply that the precursor, by itself, did not assemble. Within the minute after the addition of EDC, the concentration anhydride increased rapidly, while the concentration EDC decayed. Confocal microscopy, cryo-TEM, and turbidity measurements showed that the anhydride immediately started assembling into small vesicles. NMR experiments showed that the assemblies were a mixture of the precursor and product throughout the entire cycle which was supported by molecular simulations that revealed a subtle balance between the anhydride and precursor is required to form a stable membrane. Early in the cycle, the vesicles were multi-lamellar and ill-defined, which may be a result of the rapid increase of the anhydride concentration. After 5 minutes, the activation of the building block was slower than its deactivation, and the concentration building block was thus decreasing. The decrease in building blocks was also clear from the evolution of the turbidity and the evolution of the number of particles as counted by confocal microscopy, *i.e.*, all measurements showed the number of vesicles decreased after roughly 5 minutes. In other words, new anhydride was formed, but, because its deactivation is faster than activation, the number of vesicles is decreasing. Microscopy analysis showed that, after 5 minutes, some of the vesicles had holes in their membrane, which we explain by the deactivation of the anhydride. The kinetic model has clarified that deactivation happens both in solution and on the vesicles which further backs our hypothesis. Finally, it is currently unclear how the vesicles disassemble. We hypothesize that the holes in the vesicles become larger and that the vesicle eventually dissipate entirely.

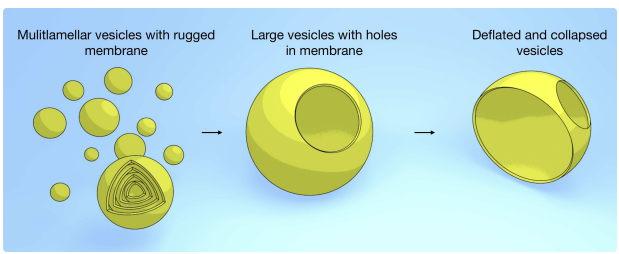

Scheme 2. Tentative mechanism of dynamic formation and decay of dissipative vesicles.

In this work, we showed the dissipative self-assembly of synthetic vesicles driven by the energy gained from the hydrolysis of a carbodiimide. These vesicles emerge in response to the addition of carbodiimide and decay when the carbodiimide runs low. As a result of the tightly coupled reaction cycle and the assembly and disassembly process, the vesicles dynamically evolve throughout the dissipative reaction cycle. That means that the vesicles are constantly remodeled by the reaction cycle. The dynamic formation of dissipative vesicles offers a new model platform to study membrane remodeling. In the future, the system could potentially help to create artificial membrane compartments.

Experimental Section

Materials

1-Ethyl-3-(3-dimethylaminopropyl) carbodiimide (EDC), 2-(*N*-morpholino)ethanesulfonic acid (MES) buffer, trifluoroacetic acid (TFA) and Nile Red were purchased from Sigma-Aldrich and used without any further purification unless otherwise indicated. Tripeptides were synthesized as described as below and all the required reagents were purchased from Sigma-Aldrich. HPLC grade acetonitrile (ACN) was purchased from VWR.

Peptide Synthesis

Peptides were synthesized using standard fluoren-9-ylmethoxycarbonyl (Fmoc) solid-phase peptide synthesis on Wang resin (100–200 mesh, 1.1 mmol/g loading). Synthesis was performed on a CEM Liberty microwave-assisted peptide synthesizer. The first amino acid coupling to the resin was accomplished by using symmetrical anhydride methodology. Briefly, a 0.2 M solution of the Fmoc-amino acid symmetrical anhydride was prepared by allowing the corresponding Fmoc-protected amino acid (FmocD(OtBu)OH or FmocE(OtBu)OH, 12 mmol) and N,N′-diisopropylcarbodiimide (DIC, 6 mmol) to react in 30 mL N,N-dimethylformamide (DMF) for 40 minutes. The solution was placed in the freezer for 15 minutes and the formed solid urea was filtered out before the next step. Loading of the resin was performed using the automated peptide synthesizer. The symmetrical anhydride solution (0.2 M, 12 mL) and 4-(dimethylamino)pyridine (DMAP) solution in DMF (20 mM, 2.5 mL) were added to the pre-swollen Wang resin (0.5 mmol, 1.1 mmol/g) and heated in the microwave (30 minutes, 75 °C). The coupling was repeated twice in order to increase the yield. The resin was then washed with DMF (2×10 mL). Before the following coupling the Fmoc protecting group was removed using a 20% solution of piperidine in DMF. The reaction mixture was heated in the microwave (1x1 minutes, 90 °C) and then washed with DMF (2×

© 2019 The Authors. Published by Wiley-VCH Verlag GmbH & Co. KGaA

10 mL). The cleavage was repeated twice. The coupling was achieved by using 4 equivalents (eq.) of Fmoc-glycine in DMF, 4 eq. of DIC and 4 eq. of ethyl (hydroxyimino)cyanoacetate (Oxyma). The resin solution was then heated in the microwave (1×2 minutes, 90 °C). This coupling was also repeated twice to increase the yield. Fmoc-cleavage and amino acid coupling were repeated as described. The tripeptide was then cleaved from the resin using a mixture (10 mL) of 50% DCM, 47.5% trifluoroacetic acid (TFA), 1.25% water, and 1.25% triisopropylsilane (TIPS) for 1.5 hours. The solvent was removed by co-distillation with ether by rotary evaporation and dried under reduced pressure. The product was purified using preparative reversed-phase high-performance liquid chromatography (HPLC, Thermofisher Dionex Ultimate 3000, Hypersil Gold 250×4.8 mm) in a linear gradient of acetonitrile (ACN with 0.1% TFA, 40% to 98%) and water (with 0.1% TFA). Purified product was lyophilized and stored at −20 °C until further use. The purity of the peptide was analysed by liquid chromatography mass spectrometry (LC–MS) as well as analytical HPLC.

Sample Preparation

Stock solutions of the precursor were prepared by dissolving the precursor in 0.2 M MES buffer, after which the pH was adjusted to pH 6.0. Stock solutions of EDC were prepared by dissolving the EDC powder in MQ water. Typically, stock solutions of 2.0 M EDC were used freshly. Reaction networks were started by addition of the high concentration EDC to the peptide solution. All analysis was carried out at 25 °C.

Kinetic Model

A kinetic model was used to predict the evolution of the anhydride concentration over time. The model is described in detail in our previous work.[32] The rate constants we used in this work are given in Table S4. The model is described in detail in supplementary notes 1. The Matlab-code we used is available here: https://github.com/BoekhovenLab/Dynamic-vesicles/

HPLC

The kinetics of the chemical reaction networks were monitored over time by means of analytical HPLC (Thermofisher Dionex Ultimate 3000, Hypersil Gold 250×4.8 mm). A 750 μL sample was prepared as described above and placed into a screw cap HPLC vial. Samples of the solutions (1.0 μL) were directly injected without further dilution and tracked with a UV/Vis detector at 220 and 254 nm. All compounds involved were separated using a linear gradient of water with 0.1% TFA to ACN with 0.1% TFA from 40:60 to 2:98 in 8 minutes.

Calibration curves for the EDC (in MQ water, λ_{abs} = 220 nm) and precursors (in 0.2 M MES buffer, λ_{abs} = 254 nm) were performed in triplicate. Calibration was not possible for the anhydrides due to their intrinsic instability. Instead, the absorption coefficient of their corresponding precursor was used. Retention times and calibration values are given in Supporting Table S1, S2 and S3.

UV/Vis Spectroscopy

The UV/Vis measurements were carried out using a Multiskan FC (Thermo Fisher) microplate reader. Samples (200 μL) were directly prepared into a 96-well plate (tissue culture plate non-treated) as described above. The data was recorded at 500 nm at 25 (±0.5) °C. We performed all measurements in triplicate.

Confocal Fluorescence Microscopy

Confocal fluorescence microscopy was performed on a Leica SP5 confocal microscope using a 63x oil immersion objective. Samples were prepared as described above, but with 2.5 μM Nile Red as dye. 20 μL of the sample was deposited on the PEG-coated glass slide and covered with a 12 mm diameter coverslip. Samples were excited with a 543 nm laser and imaged at 580–700 nm. Every 30 seconds, we acquired a 4096×4096 image of an area that covered 246×246 μm. We performed each experiment in triplicate.

Image Analysis

ImageJ's preinstalled "analyse particles" package was used to analyse the number of vesicles and their circumference under the assumption that the particles were perfectly spherical. Each data point corresponds to one image and was performed in triplicate.

Cryo-TEM

Samples for TEM were prepared as described above. The grids (C-Flat R2/2 or R4/2, 400 mesh, Cu) were freshly glow-discharged (50 mA) for 90 seconds prior to use. Preparation of the grids was performed in a FEI/Thermo Fisher Vitrobot at 25 °C with the relative humidity set to 100%. Sample (4 μL) was incubated for 30 seconds, blotted for 2.5 seconds (blotting force set to −1) and then also directly plunged into liquid ethane. The cryo-TEM grids were transferred and stored in liquid nitrogen, and when needed, placed into a Gatan cryo-transfer-specimen holder to insert into the microscope. The specimen temperature was maintained at −170 °C during the data collection. Cryo-TEM imaging was performed on a Tecnai Spirit microscope (FEI/Thermo Fisher) operating at 120 kV. The images were recorded in a low-dose mode on a CMOS camera.

LC-MS

LC–MS measurements were performed using an Agilent Technologies 1260 Infinity LC–MS system with a 6310 quadrupole spectrometer. The solvent system consisted of 0.1% formic acid in water as buffer A and 0.1% formic acid in acetonitrile as buffer B. The samples were analyzed in positive mode and followed by UV absorbance at 193, 254 and/or 280 nm.

Molecular Simulations

Coarse-grained molecular dynamics (CGMD) simulations were used to derive a molecular understanding of the assembly process of Fmoc–GGD–OH precursor/anhydride mixtures. In total 8 simulations were performed with a total length of 30 μs using Gromacs 2016.3[35] and the MARTINI 2.2 force field,[36,37] with in-house parameters developed for the precursor and anhydride. We performed quantum chemical density functional theory (DFT) calculations at the B3LYP–D3/def2-TZVP level,[38–41] performed using TURBOMOLE v. 7.2[42] to validate the relative well-depth and anisotropic interactions between Fmoc molecules in the CG-models. Three CGMD self-assembly simulations were initiated based on random initial distributions of the simulation system. Additionally, we performed three simulations with a finite membrane bilayer, and two simulations with an infinite bilayer, where the edges of the bilayers were connected through periodic boundary conditions. Detailed information of the simulations setups is given in Table S5. All simulations were performed with periodic boundary condition. The systems were solvated and neutralized, and simulated at 310 K and 1 bar pressure, using an isothermal-isobaric (NpT) ensemble, and a timestep of 10 fs. A thermostat with a

© 2019 The Authors. Published by Wiley-VCH Verlag GmbH & Co. KGaA

coupling constant of $\tau_t = 1.0$ ps[43] was used together with the Parrinello-Rahman barostat[44] with coupling constant of $\tau_p = 20.0$ ps, and a compressibility of $\chi = 3.0 \times 10^{-4}$ bar^{-1}. In simulation with infinite bilayer, we employed a semi-isotropic barostat. A cut-off of 1.4 nm was used for the calculation of electrostatic and van der Waals interactions. VMD was used for analysis and visualization.[45]

Acknowledgements

This project was supported by the German Research Foundation (DFG) through CRC/SFB 235 Project 16. J.B. is grateful for funding by the Technical University of Munich-Institute for Advanced Study, funded by the German Excellence Initiative and the European Union Seventh Framework Programme under grant agreement n° 291763 and the German Research Foundation (DFG) through CRC/SFB 863 Project B11. H.D. and F.K. acknowledge funding from the German Research Foundation via the Gottfried-Wilhelm-Leibniz Program.

Conflict of Interest

The authors declare no conflict of interest.

Keywords: dynamic self-assembly · dissipative self-assembly · remodeling · self-assembly · vesicles

[1] G. van Meer, D. R. Voelker, G. W. Feigenson, *Nat. Rev. Mol. Cell Biol.* **2008**, *9*, 112–124.
[2] T. Harayama, H. Riezman, *Nat. Rev. Mol. Cell Biol.* **2018**, *19*, 281–296.
[3] Ü. Coskun, K. Simons, *Structure* **2011**, *19*, 1543–1548.
[4] B. Wang, P. Tontonoz, *Annu. Rev. Physiol.* **2018**, *81*, 1–24.
[5] C. B. Minkenberg, B. Homan, J. Boekhoven, B. Norder, G. J. M. Koper, R. Eelkema, J. H. van Esch, *Langmuir* **2012**, *28*, 13570–13576.
[6] C. B. Minkenberg, W. E. Hendriksen, F. Li, E. Mendes, R. Eelkema, J. H. van Esch, *Chem. Commun.* **2012**, *48*, 9837.
[7] C. B. Minkenberg, F. Li, P. van Rijn, L. Florusse, J. Boekhoven, M. C. A. Stuart, G. J. M. Koper, R. Eelkema, J. H. van Esch, *Angew. Chem. Int. Ed.* **2011**, *50*, 3421–3424; *Angew. Chem.* **2011**, *123*, 3483–3486.
[8] C. B. Minkenberg, L. Florusse, R. Eelkema, G. J. M. Koper, J. H. van Esch, *J. Am. Chem. Soc.* **2009**, *131*, 11274–11275.
[9] A. Seoane, R. J. Brea, A. Fuertes, K. A. Podolsky, N. K. Devaraj, *J. Am. Chem. Soc.* **2018**, *140*, 8388–8391.
[10] K. Takakura, T. Yamamoto, K. Kurihara, T. Toyota, K. Ohnuma, T. Sugawara, *Chem. Commun.* **2014**, *50*, 2190–2192.
[11] S. Zhang, *Nat. Biotechnol.* **2003**, *21*, 1171–1178.
[12] D. G. Fatouros, D. A. Lamprou, A. J. Urquhart, S. N. Yannopoulos, I. S. Vizirianakis, S. Zhang, S. Koutsopoulos, *ACS Appl. Mater. Interfaces* **2014**, *6*, 8184–8189.
[13] A. Nagai, Y. Nagai, H. Qu, S. Zhang, *J. Nanosci. Nanotechnol.* **2007**, *7*, 2246–2252.
[14] A. R. Sapala, S. Dhawan, V. Haridas, *RSC Adv.* **2017**, *7*, 26608–26624.
[15] S. A. P. van Rossum, M. Tena-Solsona, J. H. van Esch, R. Eelkema, J. Boekhoven, *Chem. Soc. Rev.* **2017**, *46*, 5519–5535.
[16] R. Merindol, A. Walther, *Chem. Soc. Rev.* **2017**, *46*, 5588–5619.
[17] A. Sorrenti, J. Leira-Iglesias, A. J. Markvoort, T. F. A. de Greef, T. M. Hermans, *Chem. Soc. Rev.* **2017**, *46*, 5476–5490.
[18] R. K. Grötsch, J. Boekhoven, *Self-Assem. Biomater.*, Elsevier, **2018**, pp. 235–250.
[19] J. Boekhoven, A. M. Brizard, K. N. K. Kowlgi, G. J. M. Koper, R. Eelkema, J. H. van Esch, *Angew. Chem. Int. Ed.* **2010**, *49*, 4825–4828; *Angew. Chem.* **2010**, *122*, 4935–4938.
[20] J. Boekhoven, W. E. Hendriksen, G. J. M. Koper, R. Eelkema, J. H. van Esch, *Science* **2015**, *349*, 1075–1079.
[21] S. Debnath, S. Roy, R. V. Ulijn, *J. Am. Chem. Soc.* **2013**, *135*, 16789–16792.
[22] J. Leira-Iglesias, A. Tassoni, T. Adachi, M. Stich, T. M. Hermans, *Nat. Nanotechnol.* **2018**, *13*, 1021–1027.
[23] M. Tena-Solsona, C. Wanzke, B. Riess, A. R. Bausch, J. Boekhoven, *Nat. Commun.* **2018**, *9*, 2044.
[24] B. Rieß, C. Wanzke, M. Tena-Solsona, R. K. Grötsch, C. Maity, J. Boekhoven, *Soft Matter* **2018**, *14*, 4852–4859.
[25] R. K. Grötsch, A. Angı, Y. G. Mideksa, C. Wanzke, M. Tena-Solsona, M. J. Feige, B. Rieger, J. Boekhoven, *Angew. Chem. Int. Ed.* **2018**, *57*, 14608–14612.
[26] R. K. Grötsch, C. Wanzke, M. Speckbacher, A. Angi, B. Rieger, J. Boekhoven, *J. Am. Chem. Soc.* **2019**, *141*, 25, 9872–9878
[27] L. Heinen, T. Heuser, A. Steinschulte, A. Walther, *Nano Lett.* **2017**, *17*, 4989–4995.
[28] L. Heinen, A. Walther, *Sci. Adv.* **2019**, 9.
[29] A. Sorrenti, J. Leira-Iglesias, A. Sato, T. M. Hermans, *Nat. Commun.* **2017**, *8*, 15899.
[30] J. Leira-Iglesias, A. Sorrenti, A. Sato, P. A. Dunne, T. M. Hermans, *Chem. Commun.* **2016**, *52*, 9009–9012.
[31] S. Maiti, I. Fortunati, C. Ferrante, P. Scrimin, L. J. Prins, *Nat. Chem.* **2016**, *8*, 725–731.
[32] M. Tena-Solsona, B. Rieß, R. K. Grötsch, F. C. Löhrer, C. Wanzke, B. Käsdorf, A. R. Bausch, P. Müller-Buschbaum, O. Lieleg, J. Boekhoven, *Nat. Commun.* **2017**, *8*, 15895.
[33] L. S. Kariyawasam, C. S. Hartley, *J. Am. Chem. Soc.* **2017**, *139*, 11949–11955.
[34] B. Rieß, C. Wanzke, M. Tena-Solsona, R. K. Grötsch, C. Maity, J. Boekhoven, *Soft Matter* **2018**, *14*, 4852–4859.
[35] M. J. Abraham, T. Murtola, R. Schulz, S. Páll, J. C. Smith, B. Hess, E. Lindahl, *SoftwareX* **2015**, *1–2*, 19–25.
[36] S. J. Marrink, H. J. Risselada, S. Yefimov, D. P. Tieleman, A. H. de Vries, *J. Phys. Chem. B* **2007**, *111*, 7812–7824.
[37] D. H. de Jong, G. Singh, W. F. D. Bennett, C. Arnarez, T. A. Wassenaar, L. V. Schäfer, X. Periole, D. P. Tieleman, S. J. Marrink, *J. Chem. Theory Comput.* **2013**, *9*, 687–697.
[38] A. D. Becke, *J. Chem. Phys.* **1993**, *98*, 5648–5652.
[39] C. Lee, W. Yang, R. G. Parr, *Phys. Rev. B* **1988**, *37*, 785–789.
[40] S. Grimme, J. Antony, S. Ehrlich, H. Krieg, *J. Chem. Phys.* **2010**, *132*, 154104.
[41] F. Weigend, R. Ahlrichs, *Phys. Chem. Chem. Phys.* **2005**, *7*, 3297.
[42] R. Ahlrichs, M. Bär, M. Häser, H. Horn, C. Kölmel, *Chem. Phys. Lett.* **1989**, *162*, 165–169.
[43] G. Bussi, D. Donadio, M. Parrinello, *J. Chem. Phys.* **2007**, *126*, 014101.
[44] M. Parrinello, A. Rahman, *J. Appl. Phys.* **1981**, *52*, 7182–7190.
[45] W. Humphrey, A. Dalke, K. Schulten, *J. Mol. Graph.* **1996**, *14*, 33–38.
[46] S. M. Morrow, I. Colomer, S. P. Fletcher, *Nat. Commun.* **2019**, *10*, 1011.

Manuscript received: September 10, 2019
Accepted manuscript online: September 13, 2019
Version of record online: ■■, ■■■

 © 2019 The Authors. Published by Wiley-VCH Verlag GmbH & Co. KGaA

COMMUNICATIONS

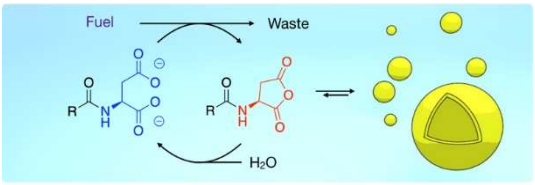

Keep it moving: The self-assembly of peptides into vesicles is coupled to a dynamic chemical reaction cycle. These vesicles emerge in response to fuel, and continuously remodel and decay when all fuel is depleted.

*C. Wanzke, A. Jussupow, F. Kohler, Prof. Dr. H. Dietz, Prof. Dr. V. R. I. Kaila, Prof. Dr. J. Boekhoven**

1 – 8

Dynamic Vesicles Formed By Dissipative Self-Assembly